

## Possible quenching of static neutron pairing near the $N = 98$ deformed shell gap: Rotational structures in $^{160,161}\text{Gd}$

D. J. Hartley<sup>1</sup>, K. Villafana,<sup>2,\*</sup> F. G. Kondev,<sup>3</sup> M. A. Riley,<sup>2</sup> R. V. F. Janssens,<sup>4,5</sup> K. Auranen,<sup>3</sup> A. D. Ayangeakaa,<sup>1,†</sup> J. S. Baron,<sup>2</sup> A. J. Boston,<sup>6</sup> M. P. Carpenter,<sup>3</sup> J. A. Clark,<sup>3</sup> J. P. Greene,<sup>3</sup> J. Heery,<sup>6</sup> C. R. Hoffman,<sup>3</sup> P. Jackson,<sup>1</sup> T. Lauritsen,<sup>3</sup> J. Li,<sup>3,‡</sup> D. Little,<sup>4</sup> E. S. Paul,<sup>6</sup> G. Savard,<sup>3</sup> D. Seweryniak,<sup>3</sup> J. Simpson,<sup>7</sup> S. Stolze,<sup>3</sup> G. L. Wilson,<sup>8</sup> J. Wu,<sup>3</sup> S. Zhu,<sup>3,§</sup> and S. Frauendorf<sup>9</sup>

<sup>1</sup>Department of Physics, U.S. Naval Academy, Annapolis, Maryland 21402, USA

<sup>2</sup>Department of Physics, Florida State University, Tallahassee, Florida 32306, USA

<sup>3</sup>Physics Division, Argonne National Laboratory, Lemont, Illinois 60439, USA

<sup>4</sup>Department of Physics and Astronomy, University of North Carolina, Chapel Hill, North Carolina 27599, USA


<sup>5</sup>Triangle Universities Nuclear Laboratory, Duke University, Durham, North Carolina 27708, USA

<sup>6</sup>Department of Physics, Oliver Lodge Laboratory, University of Liverpool, Liverpool, L69 7ZE, United Kingdom

<sup>7</sup>Nuclear Physics Group, STFC Daresbury Laboratory, Daresbury, Warrington WA4 4AD, United Kingdom

<sup>8</sup>Department of Physics and Astronomy, Louisiana State University, Baton Rouge, Louisiana 70803, USA

<sup>9</sup>Department of Physics, University of Notre Dame, Notre Dame, Indiana 46556, USA

 (Received 22 October 2020; revised 14 January 2021; accepted 11 March 2021; published 25 March 2021)

A  $^{160}\text{Gd}$  beam was accelerated to an energy of 1000 MeV and, separately, bombarded thick targets of  $^{154}\text{Sm}$  and  $^{164}\text{Dy}$  in order to observe neutron-rich, rare-earth nuclei via deep-inelastic collision processes. Gammasphere was utilized to observe  $\gamma$ -ray emissions. Many new states and transitions were observed in  $^{160}\text{Gd}$  as a result of so-called unsafe Coulomb excitation. The ground-state band in  $^{160}\text{Gd}$  has been extended to  $I^\pi = 20^+$  and a rotational band based on the  $K^\pi = 4^+$  state, previously associated with a hexadecapole vibration, was observed up to  $18^+$ . The quasiparticle configuration of the  $K^\pi = 4^+$  band has been determined, and its unusual alignment behavior may result from a possible quenching of static neutron pairing. In addition, the band based on the  $[523]5/2$  quasineutron orbital in  $^{161}\text{Gd}$  was extended from  $11/2^-$  to  $33/2^-$  and also displays the same unusual alignment behavior.

DOI: [10.1103/PhysRevC.103.034322](https://doi.org/10.1103/PhysRevC.103.034322)

### I. INTRODUCTION

Deep-inelastic collisions [1] are a well-known tool for accessing the structure of neutron-rich nuclei up to medium values of angular momentum ( $\sim 20 \hbar$ ). A recent theoretical study by Wang and Guo [2] suggested that the  $^{154}\text{Sm} + ^{160}\text{Gd}$  reaction could produce dozens of neutron-rich nuclei in the rare-earth region, many of which have no known states thus far. Therefore, by combining the capability of the ATLAS facility at Argonne National Laboratory to provide a  $^{160}\text{Gd}$  beam and the spectroscopic power of the  $\gamma$ -ray array Gammasphere, we studied this reaction, as well as the  $^{160}\text{Gd} + ^{164}\text{Dy}$  one, in attempts to possibly produce neutron-rich, rare-earth nuclei. However, for the experimental conditions under which the measurements were carried out, the “unsafe Coulomb

excitation” process, pioneered by D. Ward *et al.* [3], was dominating the cross section. As a result, the opportunity presented itself to investigate the structure of  $^{160}\text{Gd}$  as well as that of the one-neutron transfer product  $^{161}\text{Gd}$ .

The excitation of the  $^{160}\text{Gd}$  beam revealed much new information, in particular on a band structure based on the  $K^\pi = 4^+$  state at 1071 keV, which has been associated with a hexadecapole vibration [4,5]. The characteristics of this sequence were investigated through an analysis of its  $B(M1)/B(E2)$  transition strength ratios and alignment properties. Through this analysis, together with detailed cranked shell-model calculations, it is suggested that a strong reduction occurs in the static neutron pairing field due to the proximity of the  $N = 98$  deformed shell gap [6] and the blocking of specific quasineutron orbitals near this gap. Further support of the suggested reduction in pairing can be observed in the alignment behavior of the  $[523]5/2$  band in the  $N = 97$  isotones  $^{161}\text{Gd}$  and  $^{163}\text{Dy}$  [7].

### II. EXPERIMENT

The excited states of  $^{160,161}\text{Gd}$  were populated via the  $^{160}\text{Gd} + ^{154}\text{Sm}$  and  $^{160}\text{Gd} + ^{164}\text{Dy}$  reactions, where an energy of 1000 MeV was selected for the  $^{160}\text{Gd}$  beam provided by the ATLAS facility at Argonne National Laboratory. The

\*Present Address: Intel Ocotillo Campus, Chandler, AZ 85248, USA.

†Present Address: Department of Physics and Astronomy, University of North Carolina, Chapel Hill, NC 27599, USA.

‡Present Address: National Superconducting Cyclotron Laboratory, Michigan State University, East Lansing, MI 48824, USA.

§Present Address: National Nuclear Data Center, Brookhaven National Laboratory, Upton, NY 11973, USA.

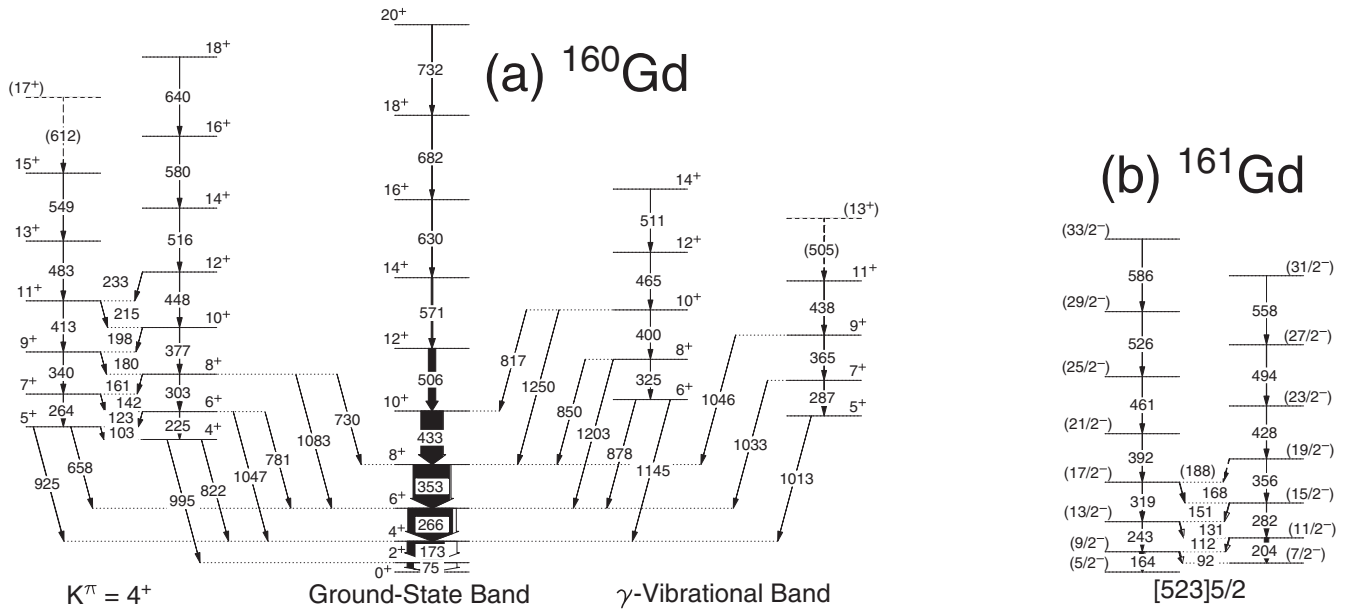


FIG. 1. Level schemes for  $^{160,161}\text{Gd}$ . Tentative transitions and levels are denoted with dashed lines. The uncertainties in energy are 0.2 keV for transitions depopulating low-energy states. However, these uncertainties become larger for transitions that depopulate increasingly higher-energy states (up to 1.5 keV for  $\gamma$  rays from the highest level) due to Doppler broadening.

chosen energy is approximately 20–25% above the Coulomb barrier. Both targets were  $\sim 240\text{--}250$  mg/cm $^2$  thick, which is sufficient to stop all of the recoils. These targets were both enriched to  $>98\%$  in their respective isotope. A beam-pulsing condition, with 412 ns between pulses, was used in order to be sensitive to possible isomer decays occurring within the beam-off periods. However, only the in-beam periods were used for the present work. The emitted  $\gamma$  rays were detected with the Gammasphere spectrometer [8] that had 73 detectors in operation at the time of these measurements. The digital Gammasphere data acquisition was used to record the multi-fold coincidence events, with a threefold trigger condition.

The in-beam data were sorted into separate coincidence cubes (one with the  $^{154}\text{Sm}$  target and the other from the  $^{164}\text{Dy}$  one) for analysis with the Radware package [9]. Coulomb excitation of the  $^{160}\text{Gd}$  beam and the target nuclei dominated the data sets; although many different species of nuclei were produced through the nucleon-transfer process, including  $^{161}\text{Gd}$ . The level schemes for  $^{160,161}\text{Gd}$  from this work are displayed in Fig. 1.

### III. LEVEL SCHEMES

Prior to this work, the most recent Coulomb excitation study of  $^{160}\text{Gd}$  [10] observed the ground-state band up to spin/parity  $16^+$ , the  $\gamma$ -vibrational band to  $(12^+)$ , and the octupole band to  $(11^-)$ . Additional levels have been observed via other reaction mechanisms, as summarized in Ref. [11]. A recent  $\beta$ -decay study [12] of  $^{160}\text{Eu}$  that feeds excited states in  $^{160}\text{Gd}$  identified the first four levels in the band labeled as  $K^\pi = 4^+$  in Fig. 1(a). In Ref. [12], the spin/parity of the lowest level of this band was assigned as  $4^+$  since it feeds the  $2^+$ ,  $4^+$ , and  $6^+$  states of the ground-state band. In addition, a determination of the internal conversion coefficient of the 103-keV

$\gamma$  ray suggests that this transition has  $M1$  character, thus, confirming the second level in the band has  $5^+$  spin and parity.

Much less was previously known about  $^{161}\text{Gd}$ . The identification of the first four levels associated with the band displayed in Fig. 1(b) was first reported in Ref. [13] based on a study of a  $(d, p)$  reaction. Approximately two decades later, the lowest three states were confirmed through the  $\beta$ -decay measurement of Ref. [14].

Although the ground-state band of  $^{160}\text{Gd}$  was extended to  $20^+$  and the  $\gamma$ -vibrational sequence to  $14^+$ , the present study will focus solely on the  $K^\pi = 4^+$  band. The spectrum of Fig. 2 displays how this band was observed to much higher spin than what had been previously published. A sum of triple coincidence gates of the 303-, 377-, 448-, and 516-keV transitions with the 822-keV  $\gamma$  ray, along with a similar sum of triple gates between 340-, 413-, 483-, and 549-keV lines with the 925-keV transition from the data set with the  $^{154}\text{Sm}$  target, produced the spectrum in Fig. 2. Note that, since both the target and the beam were Coulomb excited at the same time, many of the  $\gamma$  rays from the ground-state band in  $^{154}\text{Sm}$  are observed in the spectrum as well and these are denoted by (Sm) in Fig. 2. Doppler broadening occurs for the highest-energy transitions as a result of the recoils slowing down in the thick target. As previously mentioned, the quantum numbers of the two lowest states were determined in Ref. [12], and the spins and parities of the new levels were assigned assuming a normal rotational behavior. Therefore, this structure has now been observed up to a spin and parity of  $18^+$ .

Spectra for the structure in  $^{161}\text{Gd}$  from both the  $^{154}\text{Sm}$  and  $^{164}\text{Dy}$  data are presented in Fig. 3 to provide evidence that this sequence is, indeed, associated with this  $N = 97$  nucleus. In Fig. 3(a),  $\gamma$  rays from the  $^{154}\text{Sm}$  data set are the result of summing the triple coincidence gates of the 243-keV transition with the 461-keV one, and the 204-keV line with the

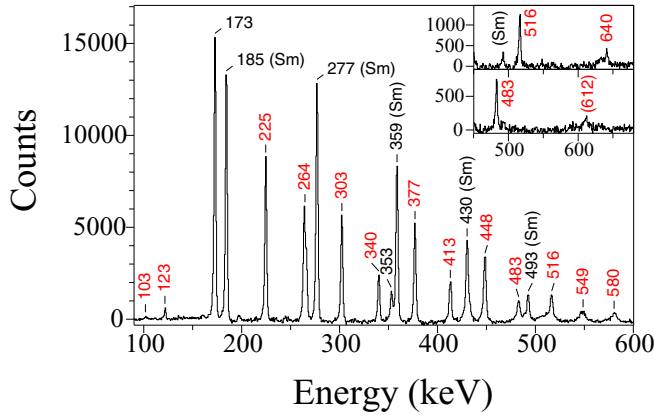


FIG. 2. Coincidence spectrum of the  $K^\pi = 4^+$  band in  $^{160}\text{Gd}$  resulting from a sum of gates (as specified in the text) in the data using a  $^{154}\text{Sm}$  target. The transitions in red are associated with the band, while those denoted with (Sm) result from the simultaneous excitation of the  $^{154}\text{Sm}$  target. Spectra in the two insets result from selected triple coincidence gates of in-band transitions with the 580-keV line for the even-spin sequence (top inset) and with the 549-keV transition for the odd-spin sequence (bottom inset) in order to display the highest transitions observed in this work.

428-keV  $\gamma$  ray. The structure seen in Fig. 1(b) can be easily observed in this spectrum and these  $\gamma$  rays are in coincidence with the 164-keV transition previously assigned to  $^{161}\text{Gd}$  [14]. Perhaps more importantly for the assignment of this sequence to  $^{161}\text{Gd}$  are the coincident transitions observed in Fig. 3(a) which are associated with  $^{153}\text{Sm}$  [15,16]. In order to produce  $^{161}\text{Gd}$ , a neutron from the  $^{154}\text{Sm}$  target must be transferred to the beam, leaving  $^{153}\text{Sm}$  as the reaction partner product with  $^{161}\text{Gd}$ . There is also evidence of  $^{152}\text{Sm}$  transitions resulting from reactions where one neutron was transferred to the beam, and a second one was released from the compound system, likely as a result of evaporation. In view of the target thicknesses involved in these measurements, Coulomb excitation of  $^{154}\text{Sm}$  and  $^{160}\text{Gd}$  dominate the reaction cross sections and this process generates a number of random coincidence events sufficient to represent a sizable background in most spectra under analysis.

A complementary spectrum from the  $^{164}\text{Dy}$  data is given in Fig. 3(b), produced under the same coincidence conditions as those used in Fig. 3(a). The same  $^{161}\text{Gd}$  transitions are observed; however,  $\gamma$  rays from  $^{163}\text{Dy}$  [7] are now found to be in coincidence with this sequence. This is evidence that the same one-neutron transfer occurred with both targets. With the same reaction mechanism observed in two separate experiments leading to the same  $\gamma$ -ray sequence, the structure shown in Fig. 1(b) can be confidently assigned to  $^{161}\text{Gd}$ . The spins of the states are based on previous assignments to the four lowest levels [13], and a rotational behavior was assumed for the assignments to higher-lying levels.

#### IV. DISCUSSION

The quasiparticle configuration for the band in  $^{161}\text{Gd}$  will be addressed first as its assignment is necessary before a

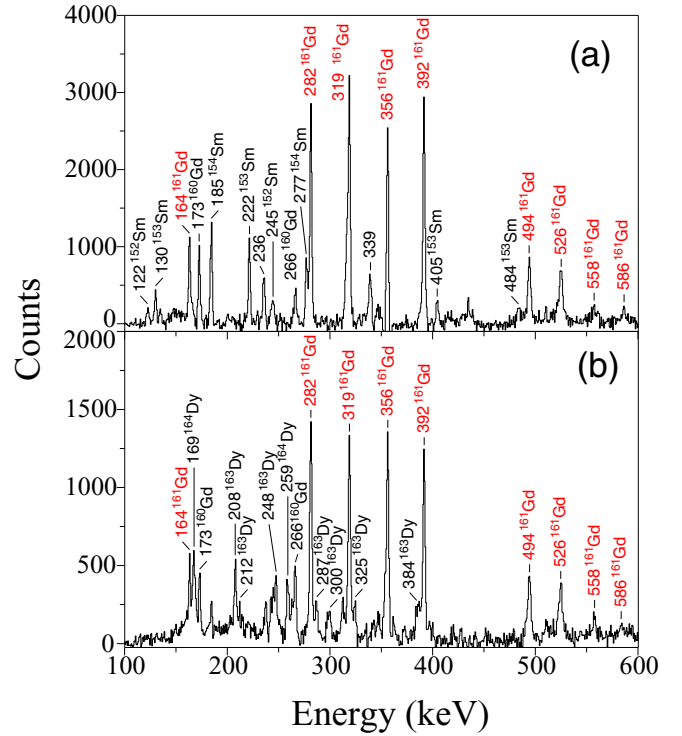


FIG. 3. Spectra displaying the sequence assigned to  $^{161}\text{Gd}$ . In panel (a), transitions from the  $^{154}\text{Sm}$  data are shown resulting from the summed coincidence gates specified in the text. In panel (b), a spectrum using the same coincidence conditions as those for panel (a), but from the  $^{164}\text{Dy}$  data is displayed.

discussion of the  $K^\pi = 4^+$  sequence in  $^{160}\text{Gd}$ . The ground-state spin and parity of  $^{161}\text{Gd}$  was previously assigned as  $5/2^-$  and was associated with the [523]5/2 quasineutron orbital due to its allowed  $\beta$  decay into the 417-keV level of  $^{161}\text{Tb}$  which is based on an  $h_{11/2}$  quasiproton [17]. In the  $N = 97$  isotone,  $^{163}\text{Dy}$ , Minehara *et al.* [18] were able to assign the [523]5/2 configuration to the ground-state structure via a comparison of experimental  $B(M1)/B(E2)$  strength ratios with theoretical calculations.

A comparison of the known [523]5/2 sequences in  $^{159}\text{Sm}$  [19,20] and  $^{163}\text{Dy}$  with the structure in  $^{161}\text{Gd}$  is given in Fig. 4. Note that the energy levels of all three structures are nearly identical, which supports the [523]5/2 assignment of the band in  $^{161}\text{Gd}$ . In addition, the nearly identical sequences suggest that all three nuclei have similar deformation.

Additional evidence for the [523]5/2 assignment can be ascertained from the  $B(M1)/B(E2)$  ratios that were calculated using the measured branching ratios ( $\lambda$ ) and the equation:

$$\frac{B(M1 : I \rightarrow I - 1)}{B(E2 : I \rightarrow I - 2)} = 0.697 \frac{1}{\lambda(1 + \delta^2)} \frac{E_\gamma^5(E2)}{E_\gamma^3(M1)},$$

where the unit for the  $\gamma$ -ray energies are in MeV. The mixing ratios,  $\delta$ , of many  $\Delta I = 1$  transitions were measured for the [523]5/2 band in  $^{163}\text{Dy}$  [18] and found to be  $\delta \approx 2$ . It was assumed that similar mixing ratios are likely in the  $^{161}\text{Gd}$  sequence, and therefore this value of  $\delta$  was used in the calculation of the experimental  $B(M1)/B(E2)$  ratios, which are

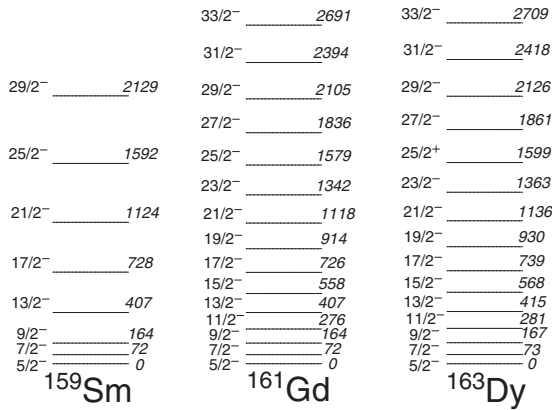


FIG. 4. Energy levels of bands based on the  $[523]5/2$  quasineutron orbital in the  $N = 97$  isotones  $^{159}\text{Sm}$ ,  $^{161}\text{Gd}$ , and  $^{163}\text{Dy}$ .

displayed in Table I. Note that these ratios are quite small, on the order of  $10^{-3} (\mu_N/eb)^2$ ; however, they are consistent with the values reported for the  $[523]5/2$  sequence in  $^{163}\text{Dy}$ .

Theoretical  $B(M1)/B(E2)$  ratios for the  $^{161}\text{Gd}$  band were calculated based on the geometrical approximation for  $B(M1)$  strengths [21] and the rotational form for the  $B(E2)$  reduced transition probabilities [22]. Parameters used in the calculation of the theoretical  $B(M1)/B(E2)$  ratios are listed in Table II. They were used together with the values  $g_R = 0.7 Z/A = 0.28$  and  $Q_0 = 7.3$  eb, where the latter is based on the measured quadrupole moment for  $^{160}\text{Gd}$  [23]. The  $g_\Omega$  values were determined through a Woods-Saxon calculation using a quadrupole deformation parameter of  $\beta_2 = 0.33$  (all other deformation parameters were set to zero). Due to the fact that the  $g_\Omega$  value for the  $[523]5/2$  configuration is nearly equal to  $g_R$ , the theoretical  $B(M1)$  rate is quite small as it depends on the quantity  $g_\Omega - g_R$ . Indeed, as seen in Table II, no other configuration will lead to such a small value. Combining this with the large  $B(E2)$  rate, theoretical  $B(M1)/B(E2)$  ratios on the order of  $10^{-4} (\mu_N/eb)^2$  were calculated. Even though these ratios are an order of magnitude smaller than the experimental ones, none of the other quasineutron configurations near the Fermi surface could produce such small ratios as those observed for this structure in  $^{161}\text{Gd}$ . Therefore, this provides further evidence of the sequence is best interpreted as being based on the  $[523]5/2$  quasineutron. It should be noted that the theoretical calculations in Ref. [18] were able to better reproduce the experimental values.

TABLE I. Branching ratios ( $\lambda$ ) and  $B(M1)/B(E2)$  ratios for states in the  $^{161}\text{Gd}$  sequence.

$I (\hbar)$	$\lambda$	$B(M1)/B(E2) (\mu_N/eb)^2$
9/2	3.4(2)	$6.3(4) \times 10^{-3}$
11/2	4.8(2)	$7.3(3) \times 10^{-3}$
13/2	7.2(7)	$7.3(7) \times 10^{-3}$
15/2	12(2)	$6.0(9) \times 10^{-3}$
17/2	17(2)	$5.8(7) \times 10^{-3}$

TABLE II. Parameters used in calculating the theoretical  $B(M1)/B(E2)$  values shown in Fig. 5.

Quasiparticle	$g_\Omega$	$i_x (\hbar)$
$\nu h_{9/2}[523]5/2$	0.29	0.5
$\nu f_{7/2}[521]3/2$	-0.51	0.2
$\pi g_{7/2}[413]5/2$	0.51	0.2
$\pi d_{5/2}[411]3/2$	1.86	0.5

As previously stated, the ground-state and  $\gamma$ -vibrational bands in  $^{160}\text{Gd}$  are known, and the present work has extended these sequences to slightly higher energies and spins without providing new insight into their nature. However, the  $K^\pi = 4^+$  band of Fig. 1(a) was significantly extended in this experiment and merits further discussion. This structure has been assigned as a band based on a hexadecapole vibration by both Burke [4] and Soloviev *et al.* [5]. In addition, the latter suggested that the quasiparticle configuration of the  $4^+$  bandhead is an approximately equal mixing of two  $K^\pi = 4^+$  states:  $\pi^2([413]5/2, [411]3/2)$  and  $\nu^2([523]5/2, [521]3/2)$ . Interestingly, evidence for the two-quasiproton state was recently found at 1483 keV in Ref. [6], where it likely undergoes two-state mixing with the level that is the bandhead of this  $K^\pi = 4^+$  band at 1071 keV. The quasiparticle nature of the sequence can be determined via the  $B(M1)/B(E2)$  ratios and the experimental values are presented in Fig. 5 as circles, where the mixing ratios were assumed to be zero. Note that an accurate value for the  $I = 7$  level could not be determined due to the overlap in energy of the  $E2$  transition and the 266-keV  $\gamma$  ray from the ground-state band. The theoretical ratios were calculated in the same manner as discussed

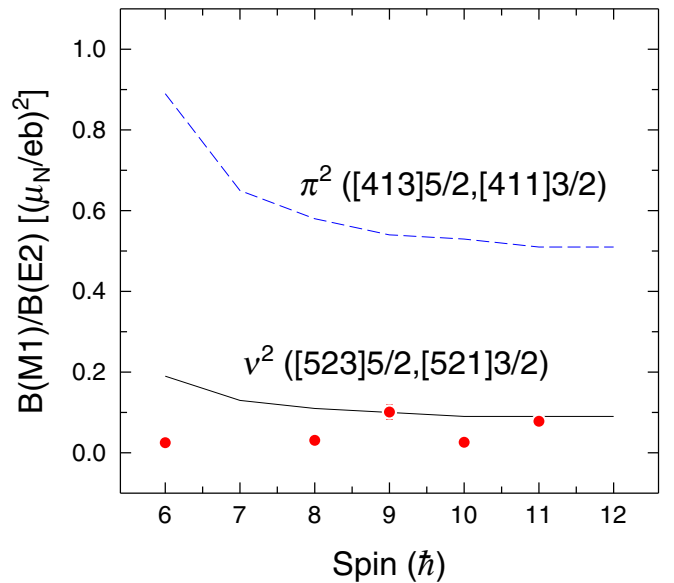


FIG. 5. Experimental and theoretical  $B(M1)/B(E2)$  strength ratios for the  $K^\pi = 4^+$  band in  $^{160}\text{Gd}$ . Parameters for the theoretical calculations are discussed in the text and given in Table II. Note that the experimental uncertainties are approximately 5–10% of the ratio value; therefore, many of the error bars are within the data points.

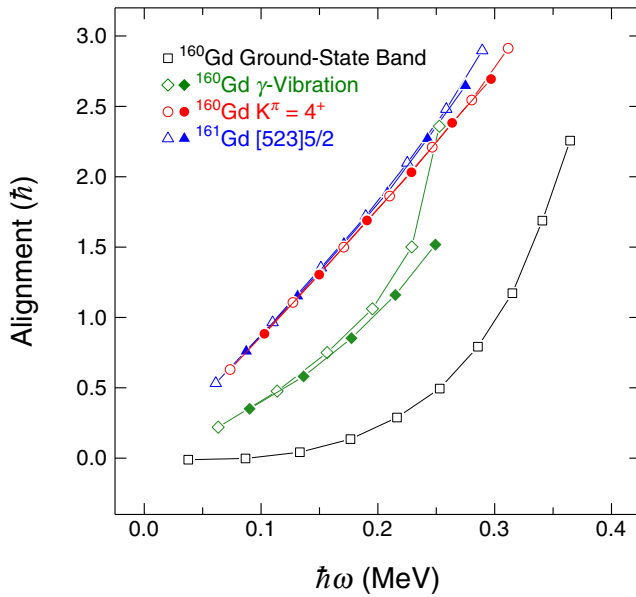


FIG. 6. Alignment of bands displayed in Fig. 1 versus rotational frequency. Note that the lower-spin states for the  $\gamma$ -vibrational band reported in Ref. [11] are included in this plot.

above for  $^{161}\text{Gd}$  using the parameters in Table II. The values for the two-quasiproton and two-quasineutron configurations are displayed in Fig. 5 as dashed and solid lines, respectively. The experimental ratios are clearly in agreement with the  $\nu^2([523]5/2, [521]3/2)$  configuration, and, therefore, the latter can be confidently assigned to this band. Note that these ratios suggest that this band has little mixing with the two-quasiproton configuration, an observation that can be contrasted with that suggested in Ref. [5]. However, it should be noted that Ref. [5] only considered the band head, while the  $B(M1)/B(E2)$  ratios presented here address the degree of mixing along the rotational sequence built on the latter state.

Figure 6 provides the alignments for the three  $^{160}\text{Gd}$  bands populated in this experiment, as well as for the  $[523]5/2$  quasineutron band in  $^{161}\text{Gd}$ . Harris parameters [24] of  $\mathcal{J}_0 = 40 \text{ } \hbar^2/\text{MeV}$  and  $\mathcal{J}_1 = 55 \text{ } \hbar^4/\text{MeV}^3$  were used to subtract the angular momentum of the rotating core. The ground-state band and the even-spin signature of the  $\gamma$ -vibrational band both display the usual behavior where, at higher rotational frequencies, an upbend is observed due to the alignment of two  $i_{13/2}$  quasineutrons. The frequency at which this occurs appears to be higher than that observed in the lighter even-even Gd isotopes. This is at least partially due to higher deformation in  $^{160}\text{Gd}$ . However, the  $K^\pi = 4^+$  sequence exhibits a remarkably constant gain of alignment as the rotational frequency increases with no indication of an upbend over the full frequency range covered by the data. As this band was associated with the  $\nu^2([523]5/2, [521]3/2)$  configuration, it would be expected to also display an upbend from the unblocked  $i_{13/2}$  alignment at the same frequency as in the ground-state band. Remarkably, the  $[523]5/2$  band in  $^{161}\text{Gd}$ , which is also plotted in Fig. 6, displays a similar constant gain in alignment, as does the  $[523]5/2$  band in  $^{163}\text{Dy}$  (see Fig. 7 in Ref. [7]). In fact, it should be noted that in Fig. 7 of Ref. [7] there is

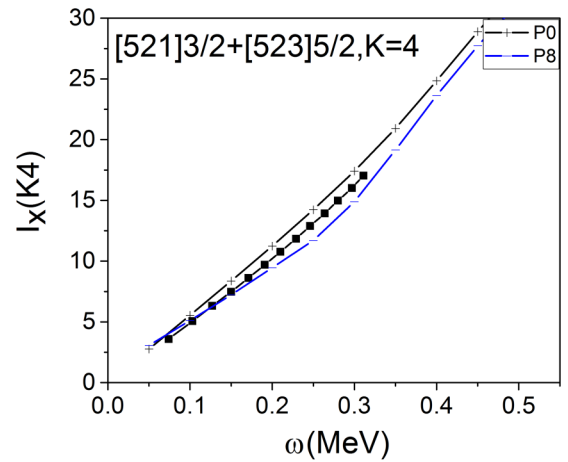


FIG. 7. The experimental aligned angular momentum (alignment) of the  $K^\pi = 4^+$  band in  $^{160}_{64}\text{Gd}$  (squares) versus rotational frequency compared with the TAC calculations assuming zero neutron pairing (P0) and a static pairing value of  $\Delta_n = 0.8 \text{ MeV}$  (P8).

a significant difference in the behavior of the alignments as a function of rotational frequency for the  $[523]5/2$  bands in  $^{161}\text{Dy}$  and  $^{163}\text{Dy}$ : While the  $i_{13/2}$  alignment is clearly present in the former, it is absent in the latter.

This unusual behavior of a constant increase in alignment was also seen in rotational bands of  $^{172,173}\text{Yb}$  [25] where the authors presented theoretical arguments that the lack of an observed crossing was likely the result of the static neutron pairing energy being essentially quenched. It is plausible that a similar argument can be made for the bands in  $^{160,161}\text{Gd}$  considered here.

In order to substantiate the possibility of a severe reduction of static neutron pairing, tilted-axis cranking (TAC) calculations [26] were performed for  $N \approx 98$  Gd, Dy, and Er nuclei. The quadrupole deformation was fixed to a value of  $\beta_2 = 0.35$  and the chemical potentials were adjusted to  $Z = 64$  and  $N = 96$ . The proton pairing energy was set to  $\Delta_p = 0.8 \text{ MeV}$  and, in each of the calculations, the protons were in their ground-state (fully paired) configuration, while the quasineutron configuration dependence on pairing was investigated.

Figure 7 compares the experimental aligned angular momentum of the  $K^\pi = 4^+$  band in  $^{160}_{64}\text{Gd}$  (without subtraction of the angular momentum associated with the core rotation) with the results of a TAC calculation in the absence of neutron pairing (denoted as P0). The smooth increase of the alignment with the rotational frequency is reproduced well with the  $\Delta = 0 \text{ MeV}$  calculation in comparison with one using a static pairing energy of  $0.8 \text{ MeV}$ , which is denoted as P8 in Fig. 7. This is an observation indicating that this structure is best represented with nearly zero static neutron pairing. The calculated moment of inertia at low  $\omega$  of  $\mathcal{J} = 55 \text{ } \hbar^2/\text{MeV}$  is somewhat larger than the experimental value of  $\mathcal{J} = 50 \text{ } \hbar^2/\text{MeV}$ . There are several possible reasons for this minor discrepancy such as a small difference in deformation or, possibly, a contribution from residual pair fluctuations. However, a study of both of these effects is beyond the scope of this paper. In order to illustrate the impact of static neutron

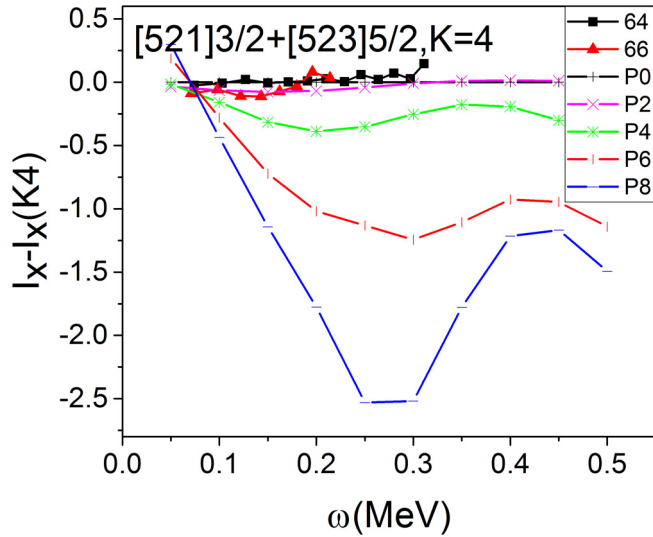


FIG. 8. The aligned angular momentum (alignment) of the  $K^\pi = 4^+$  bands in  $^{160}\text{Gd}$  and  $^{162}\text{Dy}$  [27], where a reference with the Harris parameters defined in the text was subtracted. The lines indicate the tilted-axis cranking calculations that are described in the text. The legend defines the  $Z$  of the data points, while the various colors refer to different pairing values as indicated in the legend, where P0, P2, P4, P6, and P8 refer to pairing energies of  $\Delta_n = 0, 0.2, 0.4, 0.6, 0.8$  MeV, respectively.

pairing most clearly, experimental and calculated alignments of other rotational sequences in  $^{160}\text{Gd}$  and neighboring nuclei are displayed hereafter relative to the respective alignments of the known  $K^\pi = 4^+$  bands in  $^{160}\text{Gd}$  and  $^{162}\text{Dy}$ , i.e., with a reference chosen such that the alignments of the  $K^\pi = 4^+$  bands are zero, as would be expected for a rotational band with nearly zero static pairing.

Figures 8–11 display the experimental and calculated alignments  $[I_x - I_x(K4)]$  of the  $K^\pi = 4^+$  ( $\nu([523]5/2, [521]3/2)$ ),  $[523]5/2$ , ground-state, and  $[642]5/2$  configurations, respectively. In each case, the angular momentum associated with the  $K^\pi = 4^+$  configuration  $[I_x(K4)]$  was subtracted as a reference through the use of Harris parameters [24]. For the theoretical calculations, a reference associated with the zero-pairing cranking results from the  $K^\pi = 4^+$  configuration was subtracted from the calculated angular momentum of the configurations given in each figure. In order to understand the effect of the neutron pairing field on the alignment, each figure displays the theoretical results when pairing fields of  $\Delta_n = 0, 0.2, 0.4, 0.6, 0.8$  MeV were adopted.

In Figs. 8, 9, and 10, the alignment values decrease relative to the unpaired reference as the pairing strength is increased which is due to the reduction in the moment of inertia with increasing pairing. The increase seen near  $\omega = 0.25$  MeV is a consequence of the gradual alignment of the energetically lowest  $i_{13/2}$  quasineutron pair, which is often referred to as the AB crossing. The presence of this crossing in rotational bands is evidence of the presence of a static pairing field [31]. However, as the strength of this pairing field is reduced in the calculations, this AB crossing is predicted to occur at a

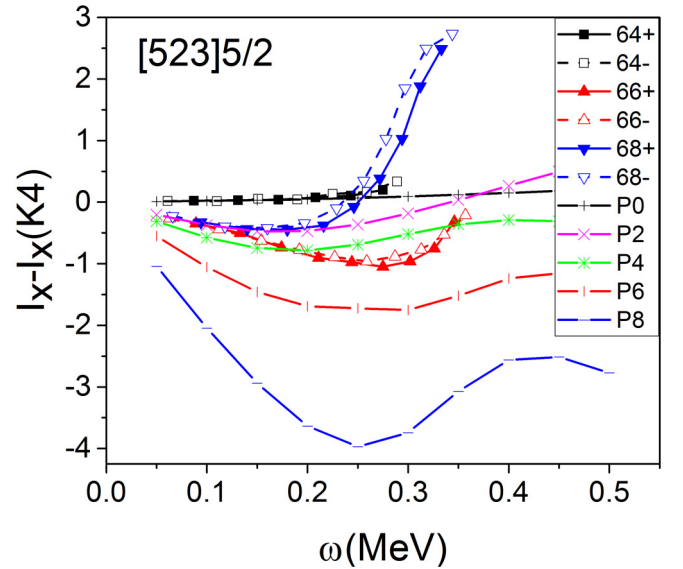


FIG. 9. Aligned angular momentum of the  $[523]5/2$  band in  $^{161}\text{Gd}$ ,  $^{163}\text{Dy}$  [7],  $^{165}\text{Er}$  [28], where the same Harris reference as the  $K^\pi = 4^+$  band was subtracted. TAC calculations using different pairing energies (as indicated in the legend in the same manner as Fig. 8) are also displayed. Full (dashed) lines are associated with the  $\alpha = +1/2$  ( $-1/2$ ) signature.

successively lower frequency, and the curves tend to flatten in the lower frequency region, below the crossing. In fact, when  $\Delta_n = 0$  MeV, the alignment curve is nearly flat and no crossing is observed. As discussed in Refs. [32,33], substantial dynamic pairing correlations are present in addition to static pairing, and these do not modify the rotational response in a qualitative way. Hence, the “zero pairing regime” does not imply that no pairing exists, but only that the mean static pairing field is zero with fluctuations about this value.

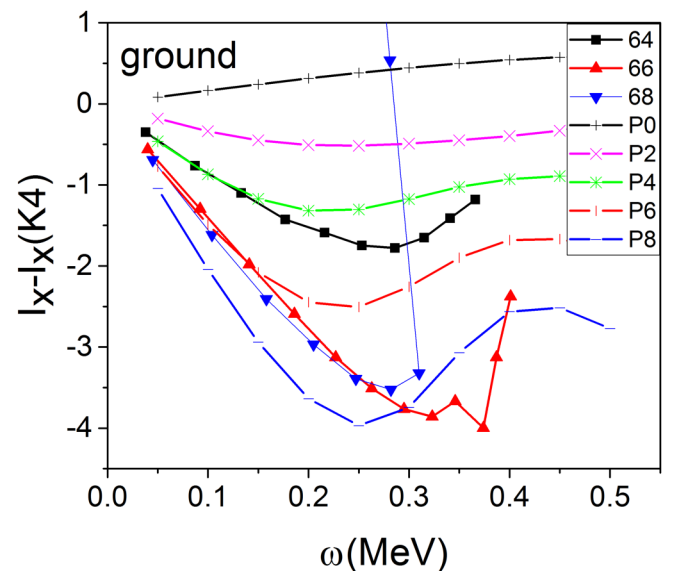


FIG. 10. Experimental and calculated alignments of the ground bands from  $^{160}\text{Gd}$ ,  $^{162}\text{Dy}$  [27], and  $^{164}\text{Er}$  [29], which were calculated and displayed in the same manner as in Fig. 8.

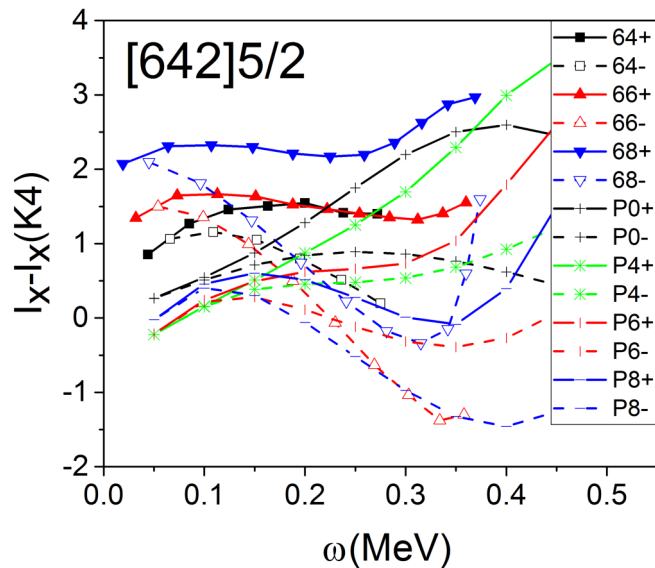


FIG. 11. Experimental and calculated alignments of the  $113/2[642]5/2$  bands from  $^{159}\text{Gd}$  [30],  $^{163}\text{Dy}$  [7], and  $^{165}\text{Er}$  [28], which were calculated and displayed in the same manner as in Fig. 9.

The experimental values of the  $K^\pi = 4^+$  configuration in  $^{160}\text{Gd}$  (Fig. 8) are clearly best represented with  $\Delta_n = 0$  MeV. In addition, the  $[523]5/2$  band in  $^{161}\text{Gd}$  (Fig. 9) is also best described in the zero pairing regime, whereas the same configuration in  $^{163}\text{Dy}$  and  $^{165}\text{Er}$  appears to have a reduced field of  $\Delta_n \approx 0.2\text{--}0.4$  MeV in the low-frequency region. The  $\Delta_n \approx 0.4$  MeV pairing calculation also appears to best reproduce the ground-state band in  $^{160}\text{Gd}$  (see Fig. 10), although a larger value of the pairing field better describes the ground-state bands in  $^{162}\text{Dy}$  and  $^{164}\text{Er}$ .

The alignment values for the  $\nu i_{13/2}$  bands from  $^{159}\text{Gd}$ ,  $^{163}\text{Dy}$ , and  $^{165}\text{Er}$  are given in Fig. 11. For these sequences, the AB crossing is Pauli blocked and, therefore, the first possible crossing involves an energetically higher pair of  $i_{13/2}$  quasineutrons (referred to as the BC crossing [31]) and occurs at a higher frequency. One may notice in Fig. 11 that the two signatures of the experimental alignments behave differently with the increase in  $\omega$ . The  $\alpha = +1/2$  sequence (solid lines) remains rather flat, while the  $\alpha = -1/2$  signature decreases as  $\omega$  increases. This difference between the signatures is observed in the TAC calculations as well; however, unlike the  $K^\pi = 4^+$  and  $[523]5/2$  configurations of  $^{160}\text{Gd}$  and  $^{161}\text{Gd}$ , respectively, the  $\Delta_n = 0$  MeV calculations do not reproduce the experimental data. Instead, the calculations with  $\Delta_n = 0.6$  or  $0.8$  MeV appear to best describe the experimental results. This suggests that configuration-dependent pairing may be present in the nuclei of this region.

The origin of this configuration-dependent pairing may be related to the fact that the negative-parity neutron orbitals ( $[523]5/2$  and  $[521]3/2$ ) retain more of their “blocking power” in comparison to the  $[642]5/2$  one. As discussed in Refs. [32,34], this power depends on the overlap of the wave functions associated with the two signatures ( $\alpha = +1/2$  and  $-1/2$ ) of a given orbital. These signatures are degenerate when the rotational frequency is zero, and the monopole

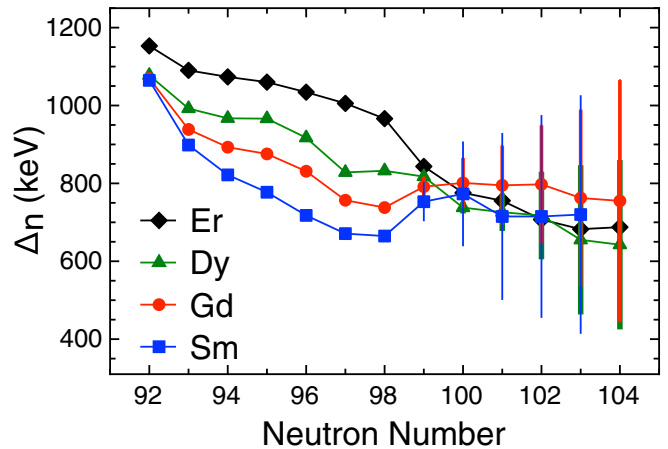


FIG. 12. Neutron pairing strength calculated from  $\Delta_n = \pm \frac{1}{4}[2S(N) - S(N-1) - S(N+1)]$ , where  $S(N)$  is the neutron separation energy. Separation energies were taken from Ref. [35].

pairing strength is assigned a value of 1. Once rotation occurs, this monopole pairing can weaken and is dependent on whether the signatures behave similarly, such that their alignment and energy values do not vary based on  $\alpha$  (no signature splitting), or whether they respond differently to the Coriolis force and thus, signature-dependent alignment and energy values are observed (signature splitting). In the former case, the blocking power is retained, and, thus if the orbital is occupied by a single quasineutron the impact on the static pairing field is significant. In contrast, in the latter case, the blocking power for the orbital is reduced and, therefore, occupation has less of an effect on the overall pairing field, as seen with the  $[642]5/2$  orbital.

It is suggested that the presence of the  $N = 98$  deformed neutron shell gap might enhance this configuration-dependent pairing effect. As seen in Fig. 5–3 of Ref. [22] the  $[523]5/2$  and  $[521]3/2$  orbitals lie just below the  $N = 98$  gap. This gap was discussed in Ref. [6], and evidence for it can be observed in Fig. 12 that plots the neutron pairing energy as measured from mass differences. Note that for Sm, Gd, and Dy the pairing energy is low at  $N = 98$  as a result of a lower density of neutron orbitals available for quasineutron pairs to scatter into. Therefore, when the two orbitals are blocked due to the  $K^\pi = 4^+$  configuration, the size of the  $N = 98$  gap effectively increases. This leads to an even lower density of states for quasineutron pairs to scatter into, thus enhancing the effect and importance of each quasineutron orbital near the Fermi surface.

Finally, it is worth mentioning that the assignment of the  $K^\pi = 4^+$  state to a hexadecapole vibrational excitation may have to be revisited in view of the discussion above. In the past, it was assumed that the excitation energy of this level (1071 keV) was too low for it to be associated with a two-quasiparticle state as this energy would usually be viewed as too small to break a pair of quasiparticles. However, with nearly vanishing static neutron pairing, this argument becomes less convincing and a low-lying, two-quasineutron configuration may be possible.

## V. SUMMARY

The level schemes of  $^{160,161}\text{Gd}$  were extended following an analysis of data resulting from reactions of a  $^{160}\text{Gd}$  beam on targets of  $^{154}\text{Sm}$  and  $^{164}\text{Dy}$ . A band based on the  $K^\pi = 4^+$  state at 1071 keV in  $^{160}\text{Gd}$  was observed up to spin 18 and its configuration of  $\nu^2([523]5/2, [521]3/2)$  was determined through a comparison of its  $B(M1)/B(E2)$  ratios with theoretical calculations. Surprisingly, this band shows no indication of an  $i_{13/2}$  crossing up to its highest observed frequency, and displays an unusually constant alignment gain over the entire range. The  $[523]5/2$  band in  $^{161}\text{Gd}$  behaves in a similar manner. The behavior of these two bands may be associated with a significant reduction in static neutron pairing. This reduction is likely the result of the proximity of these nuclei to the  $N = 98$  deformed gap and of the effect of configuration-dependent pairing.

## ACKNOWLEDGMENTS

The authors thank the ANL operations staff for their support of ATLAS and Gammasphere and gratefully acknowledge the efforts of J. P. Greene for target preparation. We thank D. C. Radford and H. Q. Jin for their software support. This work is funded by the National Science Foundation under Grants No. PHY-1907409 (USNA) and No. PHY-0754674 (FSU); the U.S. Department of Energy, Office of Nuclear Physics, under Contracts No. DE-AC02-06CH11357 (ANL), No. DE-FG02-97ER41041 (UNC), No. DE-FG02-97ER41033 (TUNL), and No. DE-FG02-95ER4093 (UND); as well as the U. K. Science and Technology Facilities Council. This research used resources of Argonne National Laboratory's ATLAS facility, which is a DOE Office of Science User Facility.

- 
- [1] R. Broda, *J. Phys. G: Nucl. Part. Phys.* **32**, R151 (2006).
- [2] N. Wang and L. Guo, *Phys. Lett. B* **760**, 236 (2016).
- [3] D. Ward, H. R. Andrews, G. C. Ball, A. Galindo-Uribarri, V. P. Janzen, T. Nakatsukasa, D. C. Radford, T. E. Drake, J. De Graaf, S. Pilotte, and Y. R. Shimizu, *Nucl. Phys. A* **600**, 88 (1996).
- [4] D. G. Burke, *Phys. Rev. Lett.* **73**, 1899 (1994).
- [5] V. G. Soloviev, A. V. Sushkov, and N. Yu. Shirikova, *Int. J. Mod. Phys. E* **6**, 437 (1997).
- [6] D. J. Hartley, F. G. Kondev, R. Orford, J. A. Clark, G. Savard, A. D. Ayangeakaa, S. Bottoni, F. Buchinger, M. T. Burkey, M. P. Carpenter, P. Copp, D. A. Gorelov, K. Hicks, C. R. Hoffman, C. Hu, R. V. F. Janssens, J. W. Klimes, T. Lauritsen, J. Sethi, D. Seweryniak, K. S. Sharma, H. Zhang, S. Zhu, and Y. Zhu, *Phys. Rev. Lett.* **120**, 182502 (2018).
- [7] A. Jungclaus, B. Binder, A. Dietrich, T. Härtlein, H. Bauer, Ch. Gund, D. Pansegrau, D. Schwalm, D. Bazzacco, E. Farnea, S. Lunardi, C. Rossi-Alvarez, C. Ur, G. de Angelis, A. Gadea, D. R. Napoli, X. R. Zhou, and Y. Sun, *Phys. Rev. C* **67**, 034302 (2003).
- [8] R. V. F. Janssens and F. S. Stephens, *Nucl. Phys. News* **6**, 9 (1996).
- [9] D. C. Radford, *Nucl. Instrum. Methods A* **361**, 297 (1995).
- [10] M. Sugawara, H. Kusakari, T. Morikawa, H. Inoue, Y. Yoshizawa, A. Virtanen, M. Piiparinen, and T. Horiguchi, *Nucl. Phys. A* **557**, 653 (1993).
- [11] C. W. Reich, *Nucl. Data Sheets* **105**, 557 (2005).
- [12] D. J. Hartley, F. G. Kondev, G. Savard, J. A. Clark, A. D. Ayangeakaa, S. Bottoni, M. P. Carpenter, P. Copp, K. Hicks, C. R. Hoffman, R. V. F. Janssens, T. Lauritsen, R. Orford, J. Sethi, and S. Zhu, *Phys. Rev. C* **101**, 044301 (2020).
- [13] P. O. Tjøm and B. Elbek, *Kgl. Danske Videnskab. Selskab, Mat.-Fys. Medd* **36**, No. 8 (1967).
- [14] H. Mach, A. Piotrowski, R. L. Gill, R. F. Casten, and D. D. Warner, *Phys. Rev. Lett.* **56**, 1547 (1986).
- [15] S. J. Asztalos, I. Y. Lee, K. Vetter, B. Cederwall, R. M. Clark, M. A. Deleplanque, R. M. Diamond, P. Fallon, K. Jing, L. Phair, A. O. Macchiavelli, J. O. Rasmussen, F. S. Stephens, G. J. Wozniak, J. A. Becker, L. A. Bernstein, D. P. McNabb, P. F. Hua, D. G. Sarantites, J. X. Saladin, C.-H. Yu, J. A. Cizewski, and R. Donangelo, *Phys. Rev. C* **60**, 044307 (1999).
- [16] T. Hayakawa, M. Oshima, Y. Hatsukawa, J. Katakura, H. Iimura, M. Matsuda, N. Shinohara, Y. S. Mitarai, T. Shizuma, M. Sugawara, and H. Kusakari, *Eur. Phys. J. A* **9**, 153 (2000).
- [17] C. W. Reich, *Nucl. Data Sheets* **112**, 2497 (2011).
- [18] E. Minehara, M. Oshima, S. Kikuchi, T. Inamura, A. Hashizume, and H. Kumahara, *Phys. Rev. C* **35**, 858 (1987).
- [19] J. K. Hwang, A. V. Ramayya, J. H. Hamilton, K. Li, C. Goodin, Y. X. Luo, J. O. Rasmussen, and S. J. Zhu, *Phys. Rev. C* **78**, 017303 (2008).
- [20] W. Urban, J. A. Pinston, G. S. Simpson, A. G. Smith, J. F. Smith, T. Rzaca-Urban, and I. Ahmad, *Phys. Rev. C* **80**, 037301 (2009).
- [21] F. Dönau, *Nucl. Phys. A* **471**, 469 (1987).
- [22] A. Bohr and B. R. Mottelson, *Nuclear Structure*, Vol. II (Benjamin, New York), 1975.
- [23] N. J. Stone, *At. Data Nucl. Data Tables* **111–112**, 1 (2016).
- [24] S. M. Harris, *Phys. Rev.* **138B**, 509 (1965).
- [25] Ts. Venkova, W. Gast, R. M. Lieder, D. Bazzacco, G. de Angelis, E. O. Lieder, A. A. Pasternak, R. Menegazzo, S. Lunardi, C. Rossi Alvarez, C. Ur, T. Martinez, M. Axiotis, D. Napoli, W. Urban, T. Rzaqca-Urban, and S. Frauendorf, *Eur. Phys. A* **26**, 19 (2005).
- [26] S. Frauendorf, *Nucl. Phys. A* **677**, 115 (2000).
- [27] C. Y. Wu, D. Cline, M. W. Simon, G. A. David, R. Teng, A. O. Macchiavelli, and K. Vetter, *Phys. Rev. C* **64**, 064317 (2001).
- [28] S. T. Wang, X. H. Zhou, Y. H. Zhang, Y. Zheng, M. L. Liu, L. Chen, N. T. Zhang, W. Hua, S. Guo, Y. H. Qiang, G. S. Li, B. Ding, Y. Shi, and F. R. Xu, *Phys. Rev. C* **84**, 017303 (2011).
- [29] S. W. Yates, I. Y. Lee, N. R. Johnson, E. Eichler, L. L. Riedinger, M. W. Guidry, A. C. Kahler, D. Cline, R. S. Simon, P. A. Butler, P. Colombani, F. S. Stephens, R. M. Diamond,



- R. M. Ronningen, R. D. Hichwa, J. H. Hamilton, and E. L. Robinson, *Phys. Rev. C* **21**, 2366 (1980).
- [30] D. J. Hartley *et al.* (unpublished).
- [31] R. Bengtsson and S. Frauendorf, *Nucl. Phys. A* **314**, 27 (1979); **327**, 139 (1979).
- [32] R. A. Broglia, M. Diebel, S. Frauendorf, and M. Gallardo, *Phys. Lett. B* **166**, 252 (1986).
- [33] S. Frauendorf, *Fifty Years of Nuclear BCS: Pairing in Finite Systems* (World Scientific, Singapore, 2013).
- [34] E. Vigezzi, D. R. Bes, R. A. Broglia, and S. Frauendorf, *Phys. Rev. C* **38**, 1448 (1988).
- [35] M. Wang, G. Audi, F. G. Kondev, W. J. Huang, S. Naimi, and X. Xu, *Chin. Phys. C* **41**, 030003 (2017).